NAVY DEPARTMENT

THE DAVID W. TAYLOR MODEL BASIN

WASHINGTON 7, D.C.

THE USE OF HELICAL SPRINGS AS NOISE ISOLATION MOUNTS

by

Alan O. Sykes

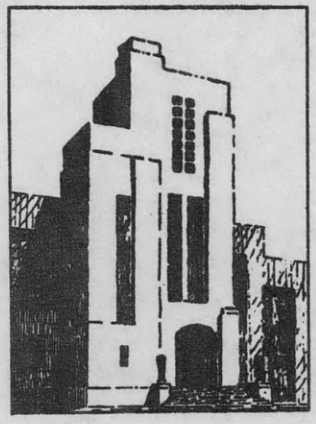

February 1952

Report 818

IN REPLY ADDRESS:
DIRECTOR, DAVID TAYLOR
MODEL BASIN, USN.

REFER TO FILE:

NAVY DEPARTMENT
DAVID TAYLOR MODEL BASIN
WASHINGTON 7, D.C.

Errata - July 1952

"The Use of Helical Springs As Noise Isolation Mounts," by Alan O. Sykes, TMB Report 818, February 1952.

Page 5. Paragraph beginning: The modulus of this expression ...
Should read: The modulus of this expression for small damping ($\omega\mu/G << 1$) at frequencies of the order of the standing wave frequencies can be shown to be:

Page 6. Equation for the phase angle: $\phi = \tan^{-1} \ldots$
Should read:

$$\phi = \tan^{-1} - \frac{\sinh n\frac{\omega l}{c}\sin\frac{\omega l}{c} + \frac{\omega l}{c}\,2\frac{M}{m}\frac{R_a^2}{a^2}\sinh n\frac{\omega l}{c}\cos\frac{\omega l}{c} + n\frac{\omega l}{c}\,2\frac{M}{m}\frac{R_a^2}{a^2}\cosh n\frac{\omega l}{c}\sin\frac{\omega l}{c}}{\cosh n\frac{\omega l}{c}\cos\frac{\omega l}{c} - \frac{\omega l}{c}\,2\frac{M}{m}\frac{R_a^2}{a^2}\cosh n\frac{\omega l}{c}\sin\frac{\omega l}{c} + n\frac{\omega l}{c}\,2\frac{M}{m}\frac{R_a^2}{a^2}\sinh n\frac{\omega l}{c}\cos\frac{\omega l}{c}}$$

INITIAL DISTRIBUTION

Copies	
17	Chief, Bureau of Ships, Project Records, Code 324, for distribution as follows: 5 Code 324 1 Code 106 8 Code 371 1 Code 344 1 Code 515 1 Code 845
2	Commanding Officer and Director, U.S. Naval Engineering Experiment Station, (Wave Mechanics), Annapolis, Md.
2	Commanding Officer and Director, U.S. Navy Underwater Sound Laboratory, Fort Trumbull, New London, Conn.
4	Director, U.S. Naval Research Laboratory, Washington 20, D.C.
2	Commanding Officer and Director, U.S. Navy Electronics Laboratory, San Diego 52, Calif.
2	Commander, Mare Island Naval Shipyard, Vallejo, Calif. 1 Rubber Laboratory 1 Code 371
1	Commander, Portsmouth Naval Shipyard, Portsmouth, N. H.
1	Director, Ordnance Research Laboratory, Pennsylvania State College, State College, Pa.
2	Commander, U.S. Naval Ordnance Laboratory, Sound Division, Silver Spring 19, Md.
2	Director, National Bureau of Standards, Washington 25, D.C.
1	Director, Acoustics Laboratory, Massachusetts Institute of Technology, Cambridge 39, Mass.
1	Director, Acoustics Laboratory, Harvard University, Cambridge, Mass.
2	Chief of Naval Research, Undersea Warfare (466)
2	Chief, Bureau of Aeronautics 1 Mr. J.E. Walsh, Jr., Room 2W80 W Bldg.)
1	Librarian, Mechanics Research Library, Illinois Institute of Technology, Technology Center, Chicago 16, Ill.

Copies

1	Mr. John D. Cooney, Associate Editor, Product Engineering, 330 West 42nd St., New York 18, N.Y.
1	Bolt Beranek and Newman, 16 Eliot St., Cambridge 38, Mass.
1	General Motors Research Division, General Motors Corp., Detroit 2, Mich. Attn: Mr. Vanator

NOTATION

A	Cross-sectional area of the spring wire
a	Radius of the spring wire
c	Velocity of shear waves in the spring wire
D_a	Mean diameter of the spring helix
d	Diameter of the spring wire
E	Effective Young's modulus of the spring
F	Weight of the mass loading the spring
F_c	Compression force acting on a plane normal to the axis of the spring wire
F_s	Shear force acting on a plane normal to the axis of the spring wire
f	Frequency
f_i	i^{th} standing-wave resonant frequency
f_o	Fundamental resonance of the mass spring system
G	Real part of the shear modulus
$\overline{G}$	Complex shear modulus = $G + i\omega\mu$
g	Acceleration of gravity
I	Moment of inertia of the mass loading the spring about the axis of the spring wire
i	$\sqrt{-1}$
K	Effective spring constant of the spring
L	Length of the spring
ℓ	Effective length of the spring wire; length of a rod in torsion with one end rigidly fixed
M	Mass of the weight loading the spring
M_b	The bending moment about an axis perpendicular to the spring wire and lying in the cylindrical surface about which the spring is wound
M_T	Moment of the force F about an axis normal to the cross section BD of the spring wire (see Figure 7)
M_t	Torsional moment about the axis of the spring wire

m	Mass of the spring
m_a	Mass of the active turns of the spring
mod	Modulus of a complex number
n	Damping parameter $n = \omega\mu/2G$
n_s	Number of active turns in the spring wire
R	Distance of a point in the spring wire from the axis of the spring
R_a	Mean radius of the spring helix
r	Radial coordinate of a point in the spring wire relative to the axis of the spring wire
$\overline{T}$	Complex transmissibility
T_{mod}	Modulus of the transmissibility
z	Coordinate of a point in the spring wire measured along the axis of the spring wire
α	Pitch angle of the spring
α_o	Attenuation per unit length of the spring wire
β_o	Phase constant per unit length of the spring wire $=\omega/c$
$\overline{\gamma}$	Complex propagation constant $= \alpha_o + i\,\beta_o$
μ	Coefficient of viscosity of the spring material
ξ	$R_a - R$
ρ	Density of the spring material
σ_c	The compressive stress in the wire due to the compressive force F_c
σ_θ	The compressive stress in the wire due to the bending moment M_b
τ_s	Shear stress due to the shear force F_s
τ_t	Shear stress due to torsion of the spring wire for a static load
$\overline{\tau}_t(r,z,t)$	Complex shear stress in a rod (the spring wire) for dynamic loading
ϕ	Phase angle of the transmissibility
ψ_o	Amplitude of the angular rotation of the spring wire at the end to which the mass is fastened
ω	$2\pi f$
ω_o	$2\pi f_o$
ω_1	$2\pi f_1$

THE USE OF HELICAL SPRINGS AS NOISE ISOLATION MOUNTS

by

Alan O. Sykes

INTRODUCTION

For numerous applications, e.g., at high temperatures or in places where rubber might deteriorate due to the presence of oils or gases, helical spring mounts offer definite advantages from the mechanical point of view.

Unfortunately, from the point of view of noise isolation, they are usually inferior to either rubber shear or compression mounts, particularly at frequencies above a few hundred cycles per second.

Because of their distributed mass, actual springs act as ideal springs only at low frequencies and wave effects occur at higher frequencies. These effects may either increase or decrease the isolation depending on both the damping* and the frequency.

At certain frequencies standing wave resonances occur and at these frequencies isolation depends on the damping and on the ratio of the mass loading the mount to the mass of the mount. If the damping is large, the isolation is not seriously decreased compared with an ideal spring mount having the same stiffness, and may even be improved. If it is small, the mount may either isolate poorly or perhaps even amplify the exciting force.

Rubber mounts can usually be designed so that the standing wave resonances occur at high frequencies at which the damping is large. For springs the situation is different. The damping does not depend strongly on frequency and usually it is very much smaller than that of rubber. Even

---

*By damping is meant in particular the damping parameter n which is defined later in this report.

the high damping capacity metals, the copper manganese alloys, have lower damping for small stresses than many rubber materials.

Springs have two other disadvantages. Whereas ideally simple shear and compression mounts have but one mode of energy propagation, helical springs with finite pitch angles necessarily have at least two. The mode which is important at low frequencies is due to torsion of the spring wire. It can be described formally in the same fashion as the only mode of the shear and compression mounts. The mode which is important at high frequencies is due to a bending of the spring wire and has quite a different description. It is this mode which is responsible for the isolation provided by the spring not improving at high frequencies as it does for shear and compression mounts.

An additional disadvantage results from the fact that for a given stiffness, the ratio of stiffness to mass for a practical metallic spring is smaller than for a rubber spring. This implies that the standing wave frequencies will necessarily be lower.

This report presents the results of an experimental study of five copper manganese and one steel spring and summarizes the theoretical work which has been completed.

EXPERIMENTAL STUDIES

Transmissibility versus frequency recordings have been made for five copper manganese and one steel spring. The physical description of the springs may be found in Table 1. A photograph showing all six springs is listed as Figure 10. Figure 11 shows the springs coated with automobile undercoating.

From the transmissibility recordings (Figures 1 through 6), it is evident that wave phenomena play an important part in determining the characteristics of springs as noise isolation mounts.

The spring at low frequencies (perhaps below 500 cps) acts essentially as a rod in torsion (see Figure 7). On the basis of this assumption, the transmissibility may be computed. A comparison of the measured and computed standing-wave resonant frequencies may be made by examining Table 2. The agreement between the theoretical and experimental values is reasonably close for the longer springs; it is less satisfactory for the shorter ones. The calculations are apt to be in error because of the uncertainty in the number of active turns in the spring. The damping at the standing wave resonances was not computed for reasons which will be made clear later in the report. Transmissibility data at frequencies below 50 cps were not included as it was determined that at the fundamental resonances of the spring mass combinations, the viscous air damping was of the same order of magnitude as the spring damping.

The transmissibility curves for the longer springs (Figures 1, 3, 4, 6) may be divided roughly into three parts. Below 500 cps, the spring action can be attributed mostly to torsion of the spring wire. Between 500 cps and 1000 cps, both bending and torsion are important. At higher frequencies, bending is the most important effect.

The transmissibilities for the shorter springs (Figures 2, 5) are quite different from those of the longer ones. The torsion theory at low frequencies seems less applicable and the behavior at high frequencies is different. The difference in behavior at high frequencies is considered to result from the increased effect of rotary inertia of the wire cross section as the wire length-diameter ratio decreases.

The height of the transmissibility peaks below 500 cps is inversely proportional to the damping factor $n = \omega\mu/2G$, where μ is the coefficient of viscosity of the material, G is the real part of the shear modulus of the material, and ω is the circular frequency. Examination of the curves shows that the copper manganese springs are more damped than is the steel spring; however, the damping is still low compared to a rubber

sample or a spring coated with some damping material. This can be seen by comparing the two recordings in each of Figures 1 through 6. The top recording was made with the spring as illustrated in Figure 10. The bottom recording was made with the spring coated with fendex as in Figure 11. The damping material coating was from 1/32 in. to 1/16 in. thick.

From the increase in frequency of the standing wave resonances, it is evident that the coating increases the spring stiffness. Moreover, it damps both the torsion and bending modes in the spring (see Figures 1, 3, 4, 6). The damping effect at high frequencies for the shorter springs (Figures 2, 5) does not appear to be as great, however.

From the nature of the transmissibility curves it is evident that a spring is a complicated dynamical system and that to understand its action thoroughly, a theoretical analysis should be made. This analysis has been undertaken and the results which have been obtained are summarized in the following section of this report. Much work remains to be done.

THEORETICAL STUDIES

Analysis of an helical spring constrained to move only in the direction of the helix axis with or without rotation shows that several modes of energy propagation are possible. The means by which these modes are excited are illustrated in Figure 7.

For static loading of the spring, the total moment $M_T = F R_a$ (where F is the weight on the spring and R_a is the average spring radius) can be broken into two components, $M_t = F R_a \cos \alpha$ and $M_b = F R_a \sin \alpha$ where α is the pitch angle of the spring. The first of these moments M_t causes a torsion of the spring wire; the second M_b causes a bending of the spring wire. The total shear force F acting on a cross section BD (see Figure 7) can be broken into two forces, $F_s = F \cos \alpha$ and $F_c = F \sin \alpha$. The first of these forces F_s causes a shear perpendicular to the spring wire and the second F_c causes a compression along the axis of the spring wire.

Examination of the magnitude of these stresses[1,2] shows that if the ratio of the spring helix diameter to wire diameter is greater than 10 and the pitch angle is small, e.g., less than 10°, then torsion of the spring wire is principally responsible for the spring action. From this consideration it follows that at low frequencies the spring should act essentially as a cylindrical rod in torsion.

The complex transmissibility $\overline{T}$ of a cylindrical rod in torsion with one end secured to a rigid foundation and the other end loaded with a rigid mass has been computed. In complex form it is given by:

$$\overline{T} = \frac{1}{\cosh \overline{\gamma} l + \dfrac{\omega^2 I}{\frac{\pi}{2} a^4 \overline{G} \overline{\gamma}} \sinh \overline{\gamma} l}$$

where $\overline{\gamma}$ = complex propagation constant of the rod $= \alpha_o + i\,\beta_o$,

$\overline{G}$ = complex shear modulus of the rod,

I = moment of inertia of the mass on the end of the rod about the axis of the rod,

$\omega = 2\pi$ times the frequency,

a = the radius of the spring wire (or rod), and

l = the effective length of the spring wire (length of the rod).

This expression is similar in form to that for the transmissibility for compression waves of a long cylindrical rod[3] and can be stated in identical form by properly defining the Young's modulus of the spring E and the moment of inertia I of the load.

The modulus of this expression for small damping ($\omega\mu/G << 1$) can be shown to be:

$$T_{mod} = \frac{1}{\sqrt{1 + \left(\frac{\omega l}{c} \frac{2R^2}{a^2} \frac{M}{m}\right)^2}} \left[\frac{1}{\sinh^2 \alpha_o l + \cos^2 \beta}\right]^{1/2}$$

---

[1]References are listed on page 10.

where M = mass of the weight loading the spring,

m = mass of the spring,

c = velocity of shear waves in the spring,

$n = c/\omega\ \alpha_o \cong \omega\mu/2G$,

α_o = attenuation per unit length of the rod,

μ = viscosity coefficient of the material,

G = the real part of the shear modulus of the material,

$$\beta = \frac{\omega l}{c} + \tan^{-1} \frac{2\omega M R_a^2}{\rho c\ \pi a^2 a^2} = \beta_o l + \tan^{-1} \frac{2\omega l}{c} \frac{R_a^2}{a^2} \frac{M}{m}, \text{ and}$$

ρ = density of the spring material.

The phase angle of the transmissibility is given by:

$$\phi = \tan^{-1} [(\tanh \alpha_o l)\ (\tan \beta)]$$

The complex stress $\tau_t(r, z, t)$ in the spring (or rod) has also been computed and is a function of both the distance z along the wire measured from the rigid foundation and the distance r from the axis of the wire (or rod).

$$\overline{\tau}_t(r, z, t) = \overline{G}\,\overline{\gamma}\psi_o\, r \frac{\cosh \overline{\gamma} z}{\sinh \overline{\gamma} l} e^{i\omega t}$$

ψ_o is a real constant equal to the amplitude of the angular rotation of the end of the rod which is loaded with the mass M.

The modulus of this expression of the damping is small ($\omega\mu/G << 1$) and is given by

$$\tau(r, z)_{mod} = G \frac{\omega}{c} \psi_o r \left[\frac{\cosh^2 \alpha_o z \cos^2 \frac{\omega z}{c} + \sinh^2 \alpha_o z \sin^2 \frac{\omega z}{c}}{\sinh^2 \alpha_o l \cos^2 \frac{\omega l}{c} + \cosh^2 \alpha_o l \sin^2 \frac{\omega l}{c}} \right]^{\frac{1}{2}}$$

Examination of this expression shows that at standing wave resonances which occur for the frequencies ($\omega\mu/G << 1$),

$$f_i = \frac{i}{2}\sqrt{\frac{K}{m}} = \frac{i}{2}\frac{c}{\ell}\left(\frac{a}{\sqrt{2}}\frac{1}{R_a}\right) \qquad i = 1, 2, 3 \ldots$$

where K is the spring constant of the spring (or rod).

$$K = \frac{Gd^4}{64\, R_a^3\, n_s} = \frac{G\, a^4}{4\, R_a^3\, n_s} = \frac{G\pi a^4}{2\, R_a^2\, 2\pi R_a n_s} = \frac{G\, a^2}{2\, R_a^2}\frac{\pi a^2}{2\pi R_a n_s} = E\frac{A}{\ell}$$

where A = cross-sectional area of spring wire,

n_s = the active number of turns in the spring,

ℓ = length of spring wire, and

E = effective Young's modulus of the spring.

The stress in certain portions of the wire becomes very large. If it happens that the damping is a function of stress, then the complex shear modulus determined from transmissibility data at standing wave resonances will represent a sort of average modulus and will depend on both the length and diameter of the spring wire. At the fundamental resonance frequency f_o given by

$$f_o \cong \frac{1}{2\pi}\sqrt{\frac{K}{M}} = \frac{1}{2\pi}\frac{c}{\ell}\sqrt{\frac{m}{M}} \,,$$

the stress is nearly uniform over the length; hence the damping in this case will depend only on the diameter of the wire.

From the discussion relating to Figure 7, one sees that the various modes are coupled because of the finite pitch of the spring.

Consider now the case of a statically loaded spring. The shear stress due to the torsion of the spring wire is given in Equation 53 of Reference 1* as:

$$\tau_t = \frac{2F\, R_a \cos\alpha}{\pi a^3}\frac{r}{a}$$

---

*Wahl gives the maximum stress $\tau = \frac{r}{a}\tau_{max}$.

The shear stress due to the shear force is:

$$\tau_s = \frac{F \cos \alpha}{\pi a^2} \quad ;$$

the ratio of these stresses is:

$$\frac{\tau_s}{\tau_t} = \frac{a}{2R_a} \frac{a}{r}$$

From this last equation it is evident that the shear stress due to the torsion of the wire is greater than that due to the shear force F_s whenever $r > a^2/2R_a$. If then the ratio of wire radius to helix radius is small, the stress over most of the wire cross section is given by the formula for τ_t.

The bending stress due to the bending moment $M_b = M_T \sin \alpha$ is given by:[4]

$$\sigma_\theta = \frac{-4M_T \sin \alpha}{\pi a^4} (R_a - R)$$

where R is the distance from the helix axis to the point in the spring wire in question. The stress σ_θ is a compressive stress which changes sign at $R = R_a$. The stress due to the force F_c is a compressive stress σ_c.

The ratio of these two stresses is given by

$$\frac{\sigma_c}{\sigma_\theta} = \frac{-F \sin \alpha}{\pi a^2} \frac{\pi a^4}{4FR_a \sin \alpha} \left(\frac{1}{R_a - R} \right) = \frac{-a^2}{4R_a} \frac{1}{R_a - R}$$

hence the stress σ_θ will be larger than σ_c except when

$$\left(R_a - \frac{a^2}{4R_a} \right) < R < R_a + \frac{a^2}{4R_a} \quad ;$$

hence if $a/R_a << 1$ then the stress in the wire due to compression will be given over most of the cross section by the expression for σ_θ.

Let us compare now the torsion stress due to the moment M_t and the compressive stress σ_θ due to M_b.

$$\frac{\sigma_\theta}{\tau_t} = \frac{\dfrac{-4M \sin\alpha\,(R - r)}{\pi a^4}}{\dfrac{2M \cos\alpha\,(R - r)}{\pi a^4}} \frac{1}{\pi a^4} = -2\frac{\sin\alpha}{\cos\alpha} = -2 \tan\alpha$$

If the pitch is small, i.e., α is small, one sees that the compressive stress is much lower than the bending stress and concludes that most of the spring action is due to torsion of the wire, the bending stress σ_θ having a secondary effect and both stresses due to F_c and F_s having still smaller effects.

The dynamic situation is somewhat different. The stresses τ_t and τ_s are propagated with the same velocity so that only one mode of propagation should result, the torsion mode perturbed by the shear stress τ_s. The stresses σ_θ and σ_c are propagated with different velocities and therefore give rise to two modes, one bending mode due to σ_θ and a compression mode due to σ_c. From the discussion of the static problem one may conclude that the torsion and bending modes are the more important.

The transmissibility expression for the bending mode has been derived but calculation of the theoretical curves has not been started.

Theoretical curves for the torsion mode are given in Figures 8 and 9 for various values of n and the ratio $2R_a^2/a^2$ M/m (Reference 3).*

ACKNOWLEDGMENTS

The author extends his gratitude and thanks to Mr. Mark Harrison for his aid and encouragement in a number of fruitful discussions, and to Mr. Bradley Wallace who did the major part of the experimental work.

---

*This reference contains a large number of curves applicable to this section besides those given in Figures 8 and 9.

REFERENCES

1. Wahl, A.M., "Mechanical Springs," Penton Publishing Co., Cleveland, Ohio, 1944.

2. Göhner, O., "Ingenieur-Archiv," Vol. 1, p. 619, 1930, and Vol. 2, pp. 1 and 381, 1931.

3. Harrison, M., and Sykes, A.O., "Wave Effects in Isolation Mounts," TMB Report 766, p. 31, May 1951.

4. Timoshenko, S., "Theory of Elasticity" McGraw-Hill, 1934, p. 362, equation f.

TABLE 1 - Spring Data

Spring Number	L inches	D_a inches	Number of Turns Total	Number of Turns Active n_s	d inches	$l = 2\pi n_s \frac{D_a}{2}$ effective l inches	Specific Damping Capacity percent	m grams	M grams	M/m	K lb/in	Alloy
1	2.13	1.24	8.75	7.0	0.150	27.2	2.38	69.0	230	3.33	17.2	76% manganese
2	0.94	1.24	4.0	2.8	0.150	10.9	2.38	28.9	440	15.2	32.1	76% manganese
3	2.22	1.24	8.25	7.3	0.150	28.4	2.38	67.0	446	6.65	13.4	72% manganese
4	3.00	1.23	11.5	10.0	0.150	39.0	0.25	89.0	446	5.01	12.4	72% manganese
5	0.98	1.23	4.5	3.4	0.150	13.3	0.25	34.7	230	6.64	25.2	72% manganese
6	2.20	1.15	7.25	5.3	.178	19.3	very low	80.9	661	8.27	141.5	steel

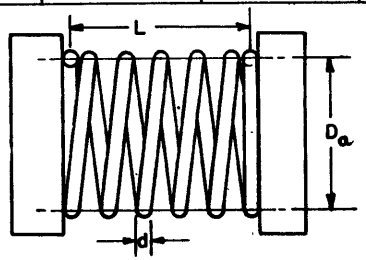

TABLE 2 - Resonant Frequencies (in cps) for the Uncoated Springs

	Spring Number 1		Spring Number 2		Spring Number 3		Spring Number 4		Spring Number 5		Spring Number 6	
	Measured	Computed	Measured	Computed	Measured	Computed	Measured	Computed	Measured	Computed	Measured	Computed
f_0	18.0	18.2	18.5	17.2	11.5	11.5	11.3	11.1	18.3	21.8	34.0	30.6
f_1	116	114	265	258	106	98.8	81	83.5	216	202	322 370	325
f_2	217	228	-	516	208	197	165	167	388	404	630 682	650
f_3	329	342	-	773	304	296	247	250	510	606	880 970	975
f_4	441	456	-	1030	406	396	312	334	645	808		1300

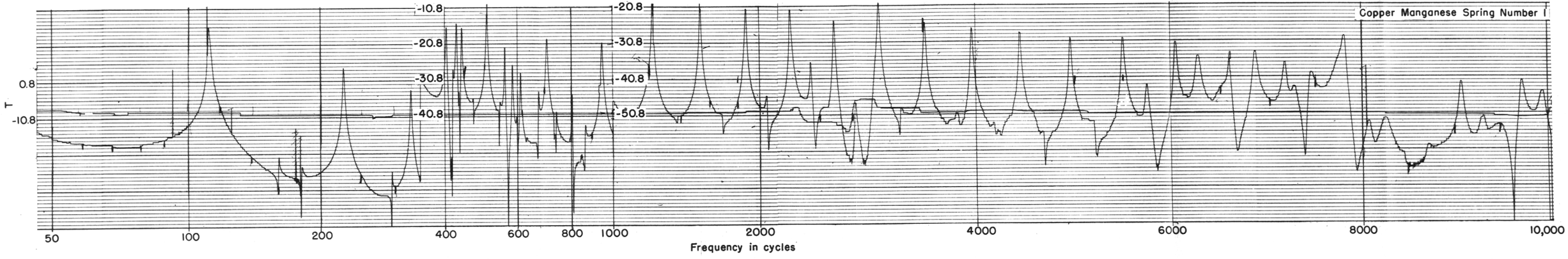
Copper Manganese Spring Number I
T
0.8
-10.8
-10.8
-20.8
-30.8
-40.8
-20.8
-30.8
-40.8
-50.8
50
100
200
400
600
800
1000
2000
4000
6000
8000
10,000
Frequency in cycles

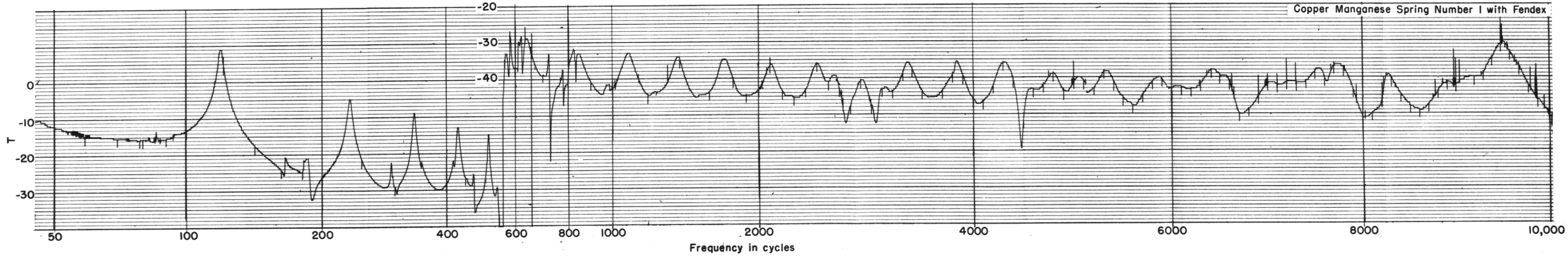
Copper Manganese Spring Number I with Fendex
T
0
-10
-20
-30
-20
-30
-40
50
100
200
400
600
800
1000
2000
4000
6000
8000
10,000
Frequency in cycles

Figure 1

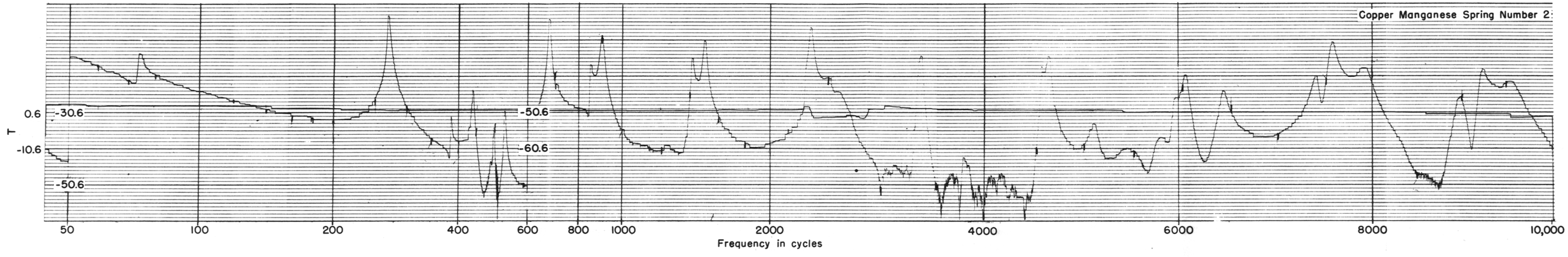
Copper Manganese Spring Number 2
T
0.6
-10.6
-30.6
-50.6
-50.6
-60.6
50
100
200
400
600
800
1000
2000
4000
6000
8000
10,000
Frequency in cycles

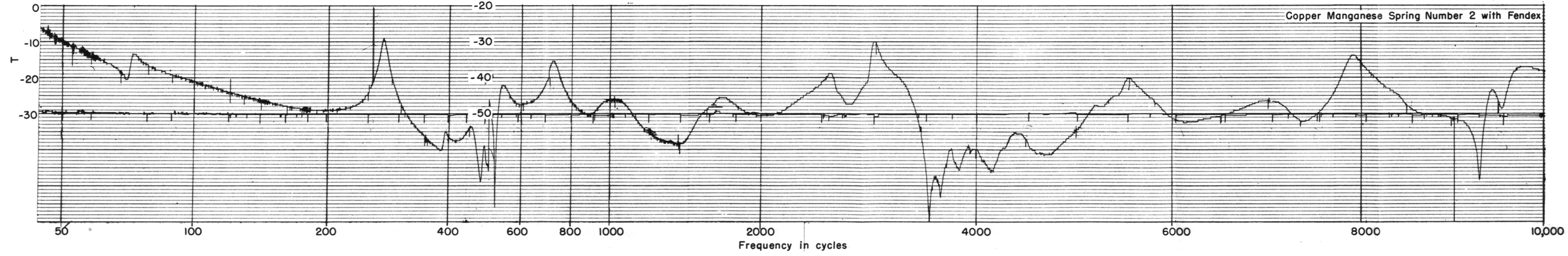
Copper Manganese Spring Number 2 with Fendex
T
0
-10
-20
-30
-20
-30
-40
-50
50
100
200
400
600
800
1000
2000
4000
6000
8000
10,000
Frequency in cycles

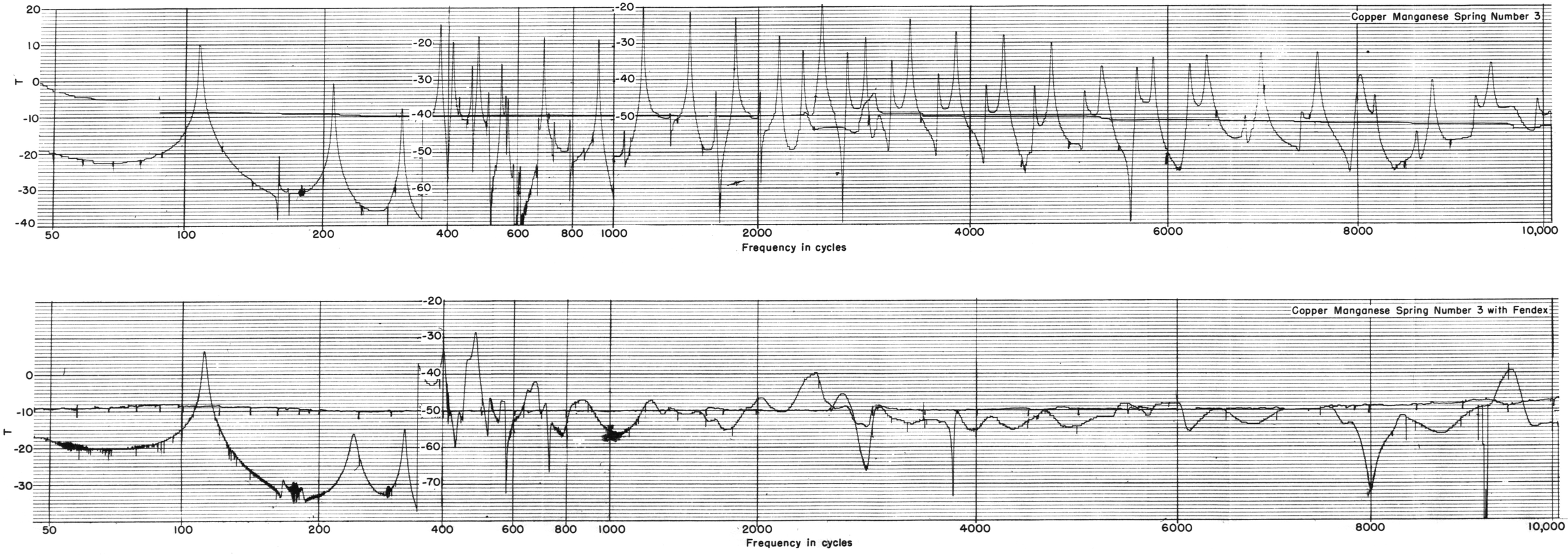
Copper Manganese Spring Number 3
T
20
10
0
-10
-20
-30
-40
-20
-30
-40
-50
-60
-20
-30
-40
-50
50
100
200
400
600
800
1000
2000
4000
6000
8000
10,000
Frequency in cycles
Copper Manganese Spring Number 3 with Fendex
T
0
-10
-20
-30
-20
-30
-40
-50
-60
-70
50
100
200
400
600
800
1000
2000
4000
6000
8000
10,000
Frequency in cycles

Figure 3

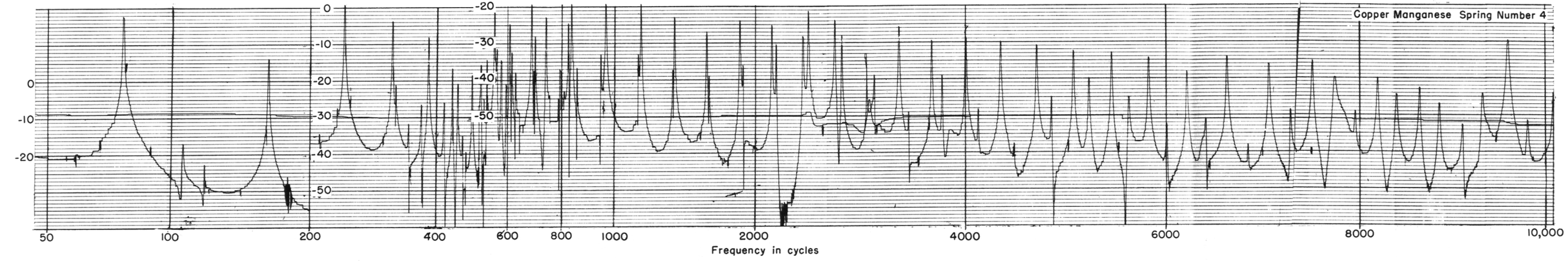
Copper Manganese Spring Number 4
0
-10
-20
-30
-40
-50
50
100
200
400
600
800
1000
2000
4000
6000
8000
10,000
Frequency in cycles

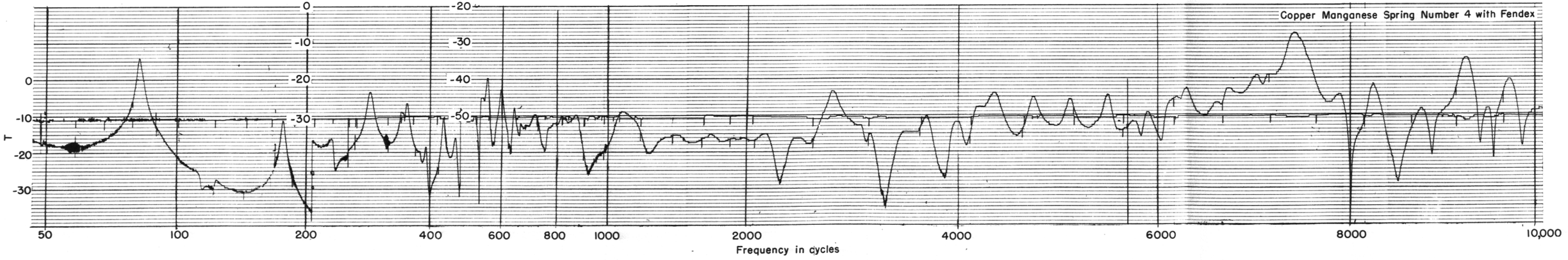
Copper Manganese Spring Number 4 with Fendex
T
0
-10
-20
-30
-40
-50
50
100
200
400
600
800
1000
2000
4000
6000
8000
10,000
Frequency in cycles

Figure 4

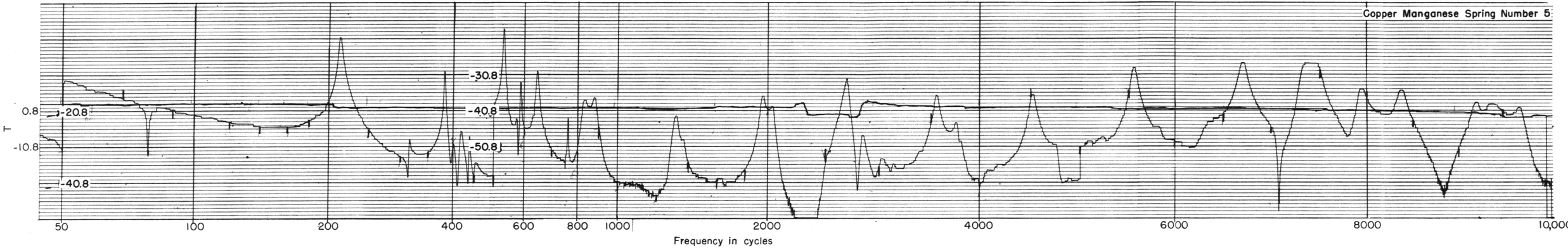
Copper Manganese Spring Number 5
T
0.8
-10.8
-20.8
-40.8
-30.8
-40.8
-50.8
50
100
200
400
600
800
1000
2000
4000
6000
8000
10,000
Frequency in cycles

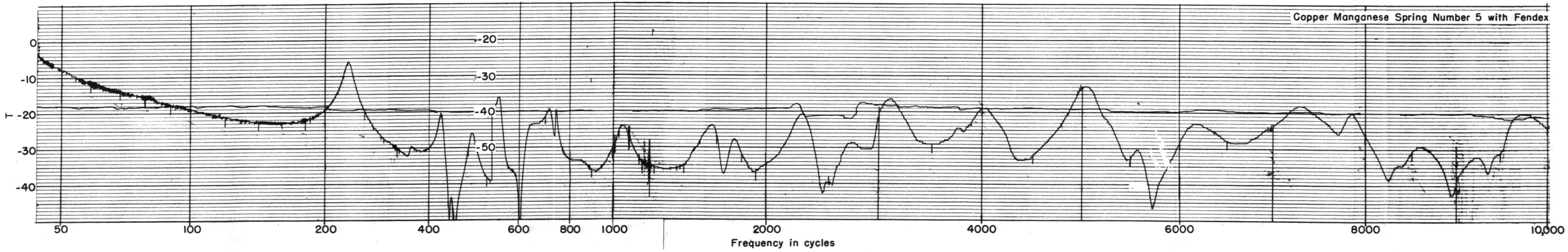
Copper Manganese Spring Number 5 with Fendex
T
0
-10
-20
-30
-40
-20
-30
-40
-50
50
100
200
400
600
800
1000
2000
4000
6000
8000
10,000
Frequency in cycles

Figure 5

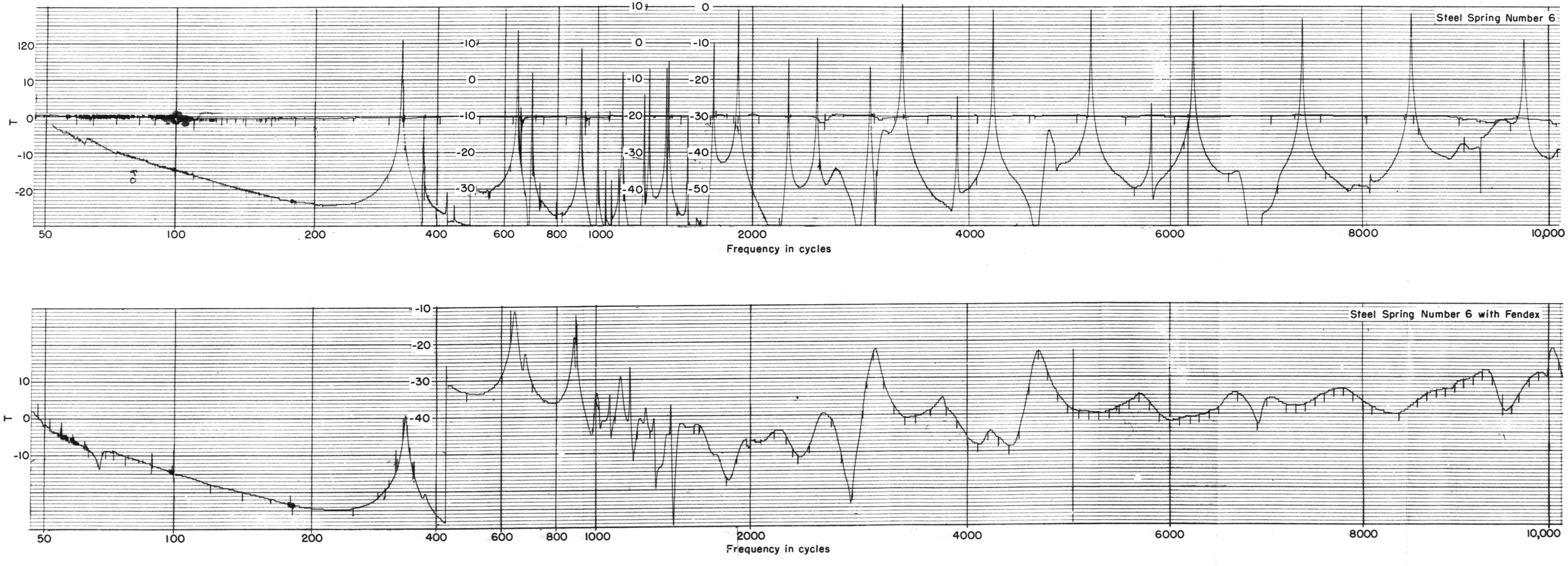
Steel Spring Number 6
T
120
10
0
-10
-20
10
0
-10
-20
-30
-40
-50
50
100
200
400
600
800
1000
2000
4000
6000
8000
10,000
Frequency in cycles
Steel Spring Number 6 with Fendex
T
10
0
-10
-10
-20
-30
-40
50
100
200
400
600
800
1000
2000
4000
6000
8000
10,000
Frequency in cycles

Figure 6

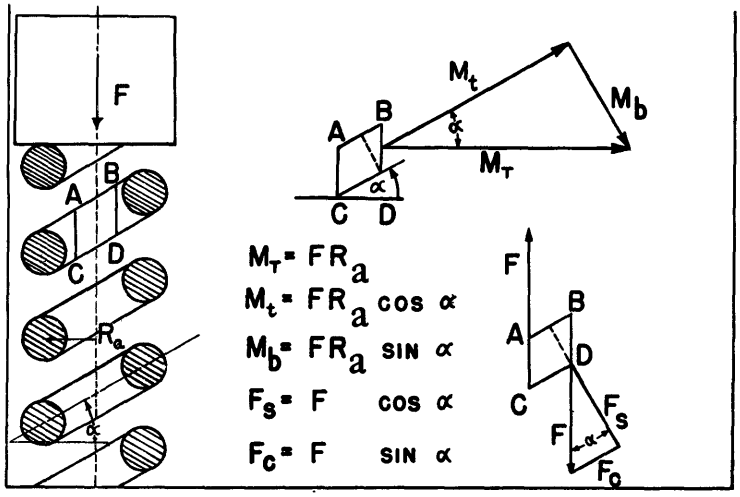

Figure 7

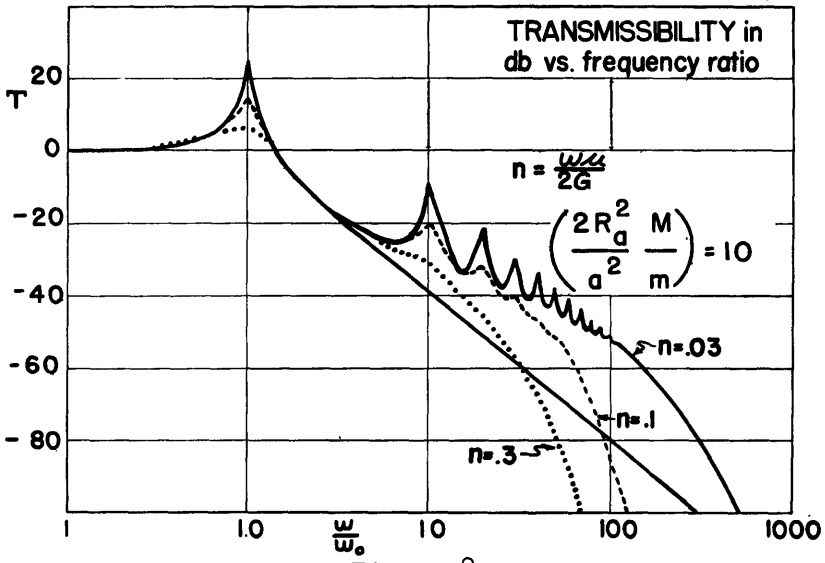

Figure 8

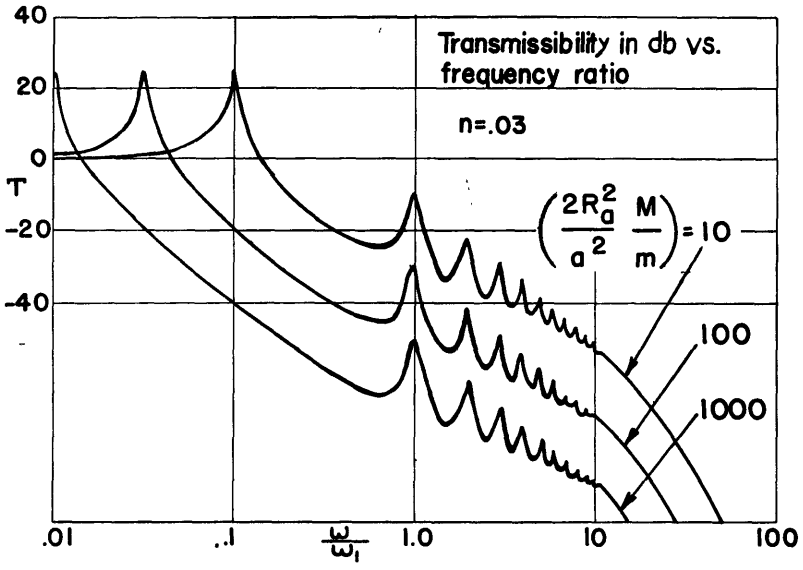

Figure 9

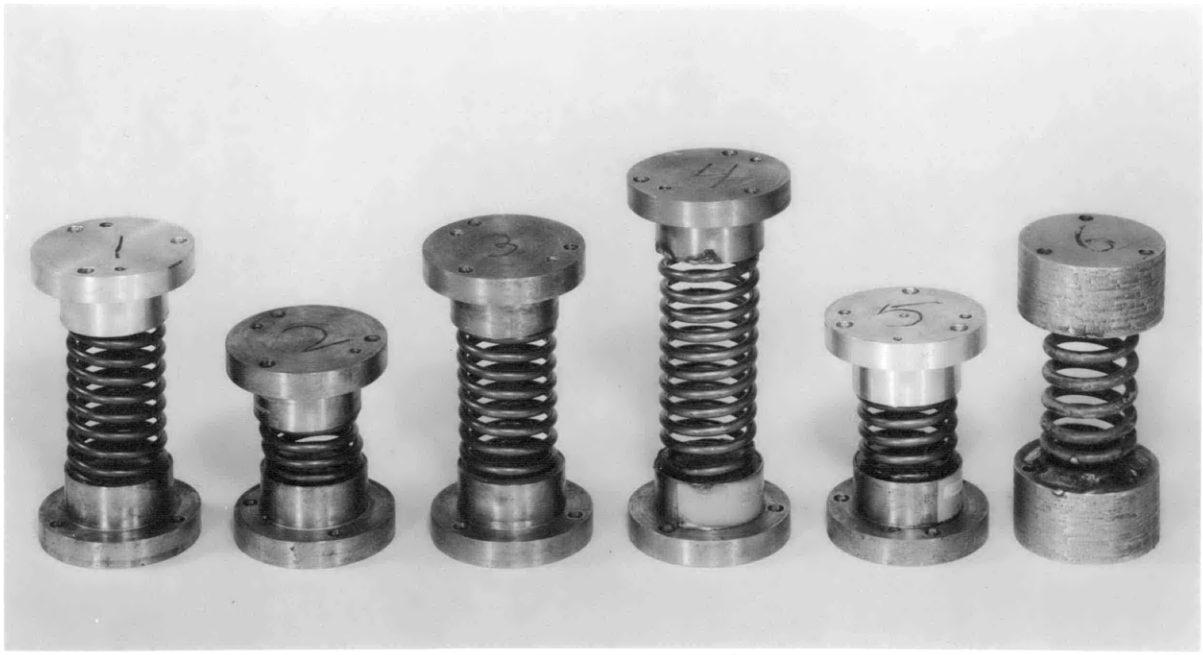

Figure 10 - Spring Specimens

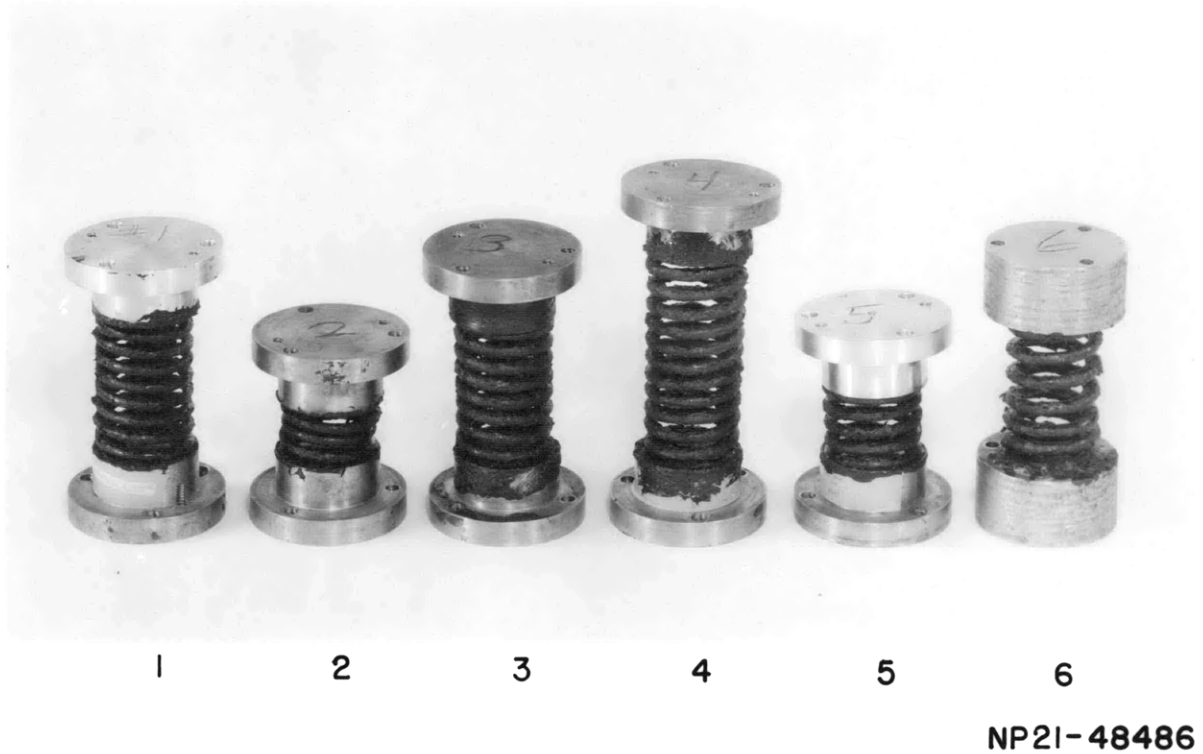

Figure 11 - Spring Specimens Coated with Fendex